NIH Public Access
Author Manuscript
Wiley Interdiscip Rev Syst Biol Med. Author manuscript; available in PMC 2014 September 01.

Published in final edited form as:
Wiley Interdiscip Rev Syst Biol Med. 2013 September ; 5(5): 643–655. doi:10.1002/wsbm.1234.

Multiscale image-based modeling and simulation of gas flow and particle transport in the human lungs

Ching-Long Lin,
The University of Iowa

Merryn H Tawhai, and
The University of Auckland

Eric A Hoffman
The University of Iowa

Ching-Long Lin: ching-long-lin@uiowa.edu

Abstract

Improved understanding of structure and function relationships in the human lungs in individuals and sub-populations is fundamentally important to the future of pulmonary medicine. Image-based measures of the lungs can provide sensitive indicators of localized features, however to provide a better prediction of lung response to disease, treatment and environment, it is desirable to integrate quantifiable regional features from imaging with associated value-added high-level modeling. With this objective in mind, recent advances in computational fluid dynamics (CFD) of the bronchial airways - from a single bifurcation symmetric model to a multiscale image-based subject-specific lung model - will be reviewed. The interaction of CFD models with local parenchymal tissue expansion - assessed by image registration - allows new understanding of the interplay between environment, hot spots where inhaled aerosols could accumulate, and inflammation. To bridge ventilation function with image-derived central airway structure in CFD, an airway geometrical modeling method that spans from the model ‘entrance’ to the terminal bronchioles will be introduced. Finally, the effects of turbulent flows and CFD turbulence models on aerosol transport and deposition will be discussed.

CFD simulation of airflow and particle transport in the human lung has been pursued by a number of research groups, whose interest has been in studying flow physics and airways resistance, improving drug delivery, or investigating which populations are most susceptible to inhaled pollutants. The three most important factors that need to be considered in airway CFD studies are lung structure, regional lung function, and flow characteristics. Their correct treatment is important because the transport of therapeutic or pollutant particles is dependent on the characteristics of the flow by which they are transported; and the airflow in the lungs is dependent on the geometry of the airways and how ventilation is distributed to the peripheral tissue. The human airway structure spans more than 20 generations, beginning with the extra-thoracic airways (oral or nasal cavity, and through the pharynx and larynx to the trachea), then the conducting airways, the respiratory airways, and to the alveoli. The airways in individuals and sub-populations (by gender, age, ethnicity, and normal vs. diseased states) may exhibit different dimensions, branching patterns and angles, and thickness and rigidity. At the local level, one would like to capture detailed flow characteristics, e.g. local velocity profiles, shear stress, and pressure, for prediction of particle transport in an airway (lung structure) model that is specific to the geometry of an individual, to understand how inter-subject variation in airway geometry (normal or pathological) influences the transport and deposition of particles. In a systems biology

Correspondence to: Ching-Long Lin, ching-long-lin@uiowa.edu.

NIH-PA Author Manuscript
NIH-PA Author Manuscript
NIH-PA Author Manuscript

NIH-PA Author Manuscript

NIH-PA Author Manuscript

NIH-PA Author Manuscript

– or multiscale modeling – approach, these local flow characteristics can be further integrated with epithelial cell models for the study of mechanotransduction. At the global (organ) level, one would like to match regional ventilation (lung function) that is specific to the individual, thus ensuring that the flow that transports inhaled particles is appropriately distributed throughout the lung model. Computational models that do not account for realistic distribution of ventilation are not capable of predicting realistic particle distribution or targeted drug deposition. Furthermore, the flow in the human lung can be transitional or turbulent in the upper and proximal airways, and becomes laminar in the distal airways. The flows in the laminar, transitional and turbulent regimes have different temporal and spatial scales. Therefore, modeling airway structure and predicting gas flow and particle transport at both local and global levels require image-guided multiscale modeling strategies.

In this article, we will review the aforementioned three key aspects of CFD studies of the human lungs: airway structure (conducting airways), lung function (regional ventilation and boundary conditions), and flow characteristics (modeling of turbulent flow and its effect on particle transport). For modeling airway structure, we will focus on the conducting airways, and review both symmetric vs. asymmetric airway models, idealized vs. CT-based airway models, and multiscale subject-specific airway models. Imposition of physiological subject-specific boundary conditions (BCs) in CFD is essential to match regional ventilation in individuals, which is also critical in studying preferential deposition of inhaled aerosols in sub-populations, e.g. normals vs. asthmatics that may exhibit different ventilation patterns. Subject-specific regional ventilation defines flow distributions and characteristics in airway segments and bifurcations, which subsequently determines the transport and deposition of aerosols in the entire lungs. Turbulence models are needed to capture the transient and turbulent nature of the gas flow in the human lungs. Thus, the advantages and disadvantages of different turbulence models as well as their effects on particle transport will be discussed. The ultimate goal of the development is to identify sensitive structural and functional variables in sub-populations of normal and diseased lungs for potential clinical applications.

AIRWAY STRUCTURE

Symmetric, asymmetric, and CT-based airway models

Symmetric tubular airway models based on Weibel's symmetric model [1] have been widely used to investigate pulmonary gas flow and particle transport in the human lungs. They include single-bifurcation models [2, 3], double-bifurcation models [4], triple-bifurcation models [5], and a 23-generation model [6]. However, the human lung is asymmetric, having two left lobes and three right lobes, and marked variability of adjacent child airway size at a bifurcation. Kim and Iglesias [3] designed an asymmetric tubular single-bifurcation model by specifying different branching angles for two daughter branches, which was later used by Balásházy and Hofmann [7]. van Ertbruggen et al. [8] constructed an asymmetric seven-generation airway model based on the asymmetric model of Horsfield [9]. That is, a tree model with branching asymmetry and branch angles as defined from cast-based studies of human airway morphometry, such that the spatial position of branches was anatomically representative. Gemci et al. [10] further extended the spatial description by building a 17-generation airway model based on the skeletonization of a human bronchial tree obtained by Schmidt et al. [11] from in vitro CT image of an adult male lung excited at autopsy. Similarly, Tian et al. [12] developed an airway model of up to 15 generations, based on the anatomical human airway cast by Yeh and Schum [13]. Limitations of these asymmetric models are that they assume circular cross-sections, and are neither subject-specific nor representative of specific sub-populations.

X-ray computed tomography (CT) remains an important non-invasive method in examining lung structure and function, and for acquiring airway geometry and regional ventilation data.

NIH-PA Author Manuscript

NIH-PA Author Manuscript

NIH-PA Author Manuscript

Airway models reconstructed from CT images can capture subject-specific geometrical features of the airways, including cartilaginous rings in the proximal airways, non-circular cross-sections and curved airway segments. CT-based airway models with various numbers of airway generations are now used by an increasing number of groups [14–18]. Due to the spatial resolution of CT, these CT-based models are currently restricted to about 10 generations, and the various models in the literature vary in terms of their resolution and therefore geometric accuracy. Obtaining a high-resolution CT-based model that is free of artefact, planar at the inlets and outlets, and with a CFD-ready mesh geometry is generally tedious and time consuming. This has limited the ability to generate large numbers of high-resolution CT-airway models for CFD analysis. However, these high-resolution models are extremely important for understanding the influence of inter-subject geometric differences on the characteristics of air flow and its potential connection to mechanotransduction. For example, in asthmatic lungs, there are local airway constrictions that increase airway resistance and create local high-speed jet flow, theoretically resulting in high local shear stress and high concentrations of irritants. This potentially accelerates airway remodelling (e.g. by increasing airway wall thickness, rigidity and narrowing) in local regions, which could subsequently further alter the flow and wall shear stress, forming a vicious cycle.

Modeling of the upper airways

Because of the complexity of the geometry of the upper airways (oral or nasal cavity to larynx), most airway CFD studies neglect this region and instead initiate flow at the trachea. Lin et al.[15] demonstrated the importance of the upper airways in establishing a turbulent laryngeal jet that influences the downstream flow and particle dispersion [19]. Flow in the upper airways tends to be transitional and turbulent. In order to properly capture the nature of the flow in this region, explicit modeling of the upper airways is essential. Stapleton et al. [20] built an average mouth-larynx upper airway model based on existing data in the archival literature and the CT images of 10 human subjects along with the observation of 5 living subjects. Kleinstreuer and Zhang [21] and Xi and Longest [22] constructed an idealized circular/elliptic model based on the anatomical data by Cheng et al. [23], whereas Lin et al.[15], Choi et al.[24] and De Backer et al.[18] used CT images to construct upper airway models. While the exact geometry and flow characteristics are important for tracking e.g. particle distribution, the effect of the upper airway can be approximated by including the larynx geometry or a local constriction at the glottis to create a turbulent laryngeal jet on inspiration [25]. In the above studies the upper airways, including the glottis, are assumed rigid. Some studies assume constant inspiratory flow conditions and some assume breathing conditions. Yin et al.[26] used the correlation between glottis opening, lung function and flow rate by Stanescu et al.[27] to estimate the time-varying glottal constriction. With inspiratory flow rate in the range of 150–342 ml/s and air volume change of ~142 ml, they estimated that the glottal cross-sectional area varies by ~9%, and glottal constriction ratio varies between 55% and 59%. Given the convective nature of the flow, the turbulent intensity would not change dramatically. On expiration, the change of the glottal area is even smaller and would have little effect on the flow in the central airways because the glottis is located on the downstream side of the flow.

For high-frequency oscillatory ventilation (HFOV) with an application to mechanically-ventilated patients, Jan et al.[28] studied flow structures experimentally in a model bifurcation in the unsteady, viscous, and convective flow regimes excluding the effect of glottal constriction. Choi et al.[24] applied CFD to investigate flow structures and convective mixing under HFOV condition in three different geometrical models: a straight tube, a single-bifurcation tube model (without glottal constriction to mimic intubation), and a CT- based human airway model.

NIH-PA Author Manuscript

NIH-PA Author Manuscript

NIH-PA Author Manuscript

Multiscale subject-specific conducting airway models

Lin et al. [29] have established a method to create a fully resolved three-dimensional (3D) mesh from the trachea to any terminal bronchioles of interest, allowing one to simulate fluid and particle transport from the model entrance to the level of lung parenchyma. The airway tree beyond CT resolution is generated by a volume filling method (VFM) developed by Tawhai et al. [30, 31]. The VFM takes the skeleton of the 3D CT-resolved central airway tree in a human subject, then generates a tree to fill the entire volume within the subject's respective five lobes. The resulting airway trees are consistent with measurements from airway casts[9, 32] and imaging studies[33], although they are only specific to the subject's lung lobe shapes and orientation of their central airways. With advances in scanners and image processing algorithms, more detailed lung structures can be resolved and segmented, e.g. higher-generation airways, sub-lobes and vessel trees. These data can be further used to improve the modeling of peripheral airways.

Figure 1 demonstrates that a subject-specific entire 1D tree can be obtained from CT images (see Fig. 1(a)) supplemented by the VFM. The entire 1D tree is marked by brown lines in Fig. 1(b). One can choose the paths from the trachea to any regions of interest, e.g., marked by the black lines in Fig. 1(b). Then by assigning airway diameters (based on average morphometric values, length-to-diameter ratios, or rate of decrease with branch order), the method can construct the corresponding 3D cylindrical baseline surface geometry as shown in Fig. 1(c). The baseline geometry can further be geometry fitted to airway surface cloud points obtained from CT image segmentation via numerical optimization [34] to recover more detailed geometrical features of the airways. The entire 3D mesh in Fig. 2(a) enlarged in Fig. 2(b) is sub-divided into a number of sub-volumes, e.g. Fig. 2(c), with associated CT-based airway measures and generation number. These sub-volumes with their corresponding boundary faces shown in Figs. 2(d) and 2(e) greatly facilitate monitoring and quantifying local transport and deposition of aerosols by generation and lobe. This sub-division capability with embedded-structure information is a key feature needed for efficiently dealing with large data sets for a population-level analysis. The local constriction at the glottis, which is essential to generate the laryngeal jet on inspiration, can be modeled using an average constriction ratio [23]. Once the surface mesh and sub-volumes are identified and defined, a CFD volume mesh can be generated automatically. The CFD mesh shown in Fig. 2(a) consists of about 1.7 million tetrahedrons and takes about 10 minutes to generate.

This airway modeling method enables generation of large 3D airways to small 3D airways (thus, 3D-3D) as shown in Fig. 1(c)) by generation as well as by path, and large 3D airways to small one-dimensional (1D) airways (thus, 3D-1D) as shown in Fig. 1(b). The 3D-3D and 3D-1D coupling approach not only allows high-fidelity CFD analyses in regions of interest, but also reduces computational cost, as well as bridges airway structure to ventilation function for subject-specific physiological BCs[29] as discussed in the next section.

LUNG FUNCTION

Boundary conditions

The distribution of flow in the airways is dependent on airway characteristics, such as asymmetry of the bronchial tree or the heterogeneity of bronchoconstriction, as well as expansion of the alveolar tissue. Regional tissue expansion is not uniform, due to non-uniform material properties and gravitational deformation of the lung tissue establishing a gradient of instantaneous tissue compliance. Accounting for such effects is however not straightforward, and hence the majority of previous studies have adopted simplifying assumptions for BCs at the 'outlets' of airway models. The common assumptions are uniform pressure, mass flow, or velocity. Regardless of BCs mass conservation is guaranteed, but the resulting regional/lobar ventilation (lung function) may not be

NIH-PA Author Manuscript

NIH-PA Author Manuscript

NIH-PA Author Manuscript

physiological and subject-specific. For example, van Ertbruggen [8] used an asymmetric Horsfield geometric model [9] that assumed uniformly distributed ventilation to impose mass flow as a BC at each outlet in their CFD analysis. Ma and Lutchen [35] used a similar Horsfield model to determine lobar flow division ratios in a CT-based airway model, and assumed uniform velocity in all outlets of the same lobe to determine the mass flow to each outlet. Corley et al.[36] applied CFD and pharmacokinetic models to study airflow and dosimetry in the image-based airways of rat, monkey and human. In their study, the inlets were imposed a constant inspiratory flow rate, and the outlets were assumed a zero pressure. They solved the convection-diffusion scalar transport equation for acrolein transport and uptake, and 1D models for mucus, epithelium, and sub-epithelial layers with diffusive flux BCs for air-tissue interface. Kabilan et al.[37] coupled 3D CFD models with lower-order ordinary differential equations (ODEs) that represent distal lung mechanics. Peripheral airway resistance can also be evaluated by image data. For example, Wongviriyawong et al.[38] used positron emission tomography (PET) and CT images of non-asthmatic and asthmatic lungs acquired at baseline and post methacholine challenge to estimate structural and functional parameters. Their approach allows linking airflow obstruction and heterogeneities in airway constriction and ventilation, and subsequently evaluating peripheral airway resistance in sub-lobar units. More sophisticated approaches account for local volume expansion. Recognizing that flow distribution to different regions of lung are not uniform, De Backer et al. [39] imposed two different pressure values at the 3D CT-resolved ending segments in the left and right lungs on steady inspiration to produce heterogeneous flow partition to the left and right lungs. More recently, the same group (De Backer et al. [18]) has used lobar volume expansion between functional residual capacity (FRC) and total lung capacity (TLC) to produce subject-specific lobar ventilation as BCs. Limitations with this approach are that it is constrained to predicting ventilation for the same posture in which imaging was acquired, and a single lobar ventilation BC does not explain heterogeneous distribution of ventilation amongst sub-lobar bronchi. One alternative approach is to use impedance of the downstream airways and tissue as BCs. For example, Gillis and Lutchen[40] proposed an impedance-based model of the human lung for prediction of flow distributions that takes into consideration heterogeneous bronchoconstriction related to impairments in the mechanical properties of the lung. Their model assumed an asymmetrical branching airway system and predicted increased heterogeneity of ventilation with increasing breathing frequency. Colletti et al.[41] developed an asymmetric-tree impedance-based model of the canine lung to study the effect of mechanical heterogeneity on the distributions of flow and pressure in the injured lung. These models could be used to provide BCs for CFD studies of diseased or injured lungs. In a more generalized and predictive approach, Tawhai et al.[42–44] developed a soft-tissue mechanics model that predicts elastic deformation of the compressible lung tissue in any posture, to provide flow or pressure BCs for a 1D tree airway model. Coupling of this method with airway CFD is challenging, but would provide a comprehensive approach to studying flow distribution in any posture. A limitation is that vertical imaging is not currently available to validate lung shape change and regional strain in the upright posture. A further limitation is that the nonlinear elastic properties of the lung tissue over large deformations remain poorly described, and the effect of pathological changes on constitutive properties is not known in any detail.

Image registration and regional ventilation

Image registration can be applied to register consecutive CT image volumes and study lung tissue expansion and contraction of human subjects over multiple breathing cycles [45–47]. In registering two images, one image is used as the reference image and the other is the floating image. The floating image is then transformed to match the reference image. The registration process generates a pointwise voxel-by-voxel displacement field between the

NIH-PA Author Manuscript

NIH-PA Author Manuscript

NIH-PA Author Manuscript

two images for various applications. Figures 3(a) and 3(b) show two volumetric scans acquired with a CT scanner during breath-holds near FRC and TLC. The displacement field between two lung volumes can be used to deform the conducting airway as color-coded in red in Figs. 3(a) and 3(b), e.g. for breathing-lung simulation [48]. Local lung volume change is calculated using the Jacobian of the transformation field. The Jacobian measures local volume expansion and contraction, which can be used in conjunction with CT number to assess regional ventilation [46, 49] and regional lung tissue mechanics [50]. Figures 3(c) and 3(d) show the distribution of regional ventilation, exhibiting the property of heterogeneity. The regional ventilation can be overlapped with the entire airway tree (e.g. Fig. 1(b)) to derive flow rate fractions for parenchymal units that enclose terminal bronchioles. These fractions can subsequently be used to determine subject-specific CFD BCs at the 3D ending airway branches via tree connectivity and mass conservation [49]. This BC is referred to as an image-based BC. Recently Yin et al.[26] extended the same technique to three CT images volumes to account for non-linearity of lung mechanics. Regardless of two- or three-volume based approaches, lung hysteresis can be modeled by a pre-determined pressure volume hysteretic relationship, but it is not subject-specific. However, the registration has been applied to 4D dynamic lung volumetric images[45], which can capture subject-specific hysteresis and can potentially provide BCs for CFD.

The image-based approach to model airflow and particle transport in the human lung is multiscale because of the coupling between airways and lung parenchyma via image registration and between large and small airways via the 3D-3D and 3D-1D meshing technique. 3D provides detailed solutions at a local level, e.g. accurate prediction of hot spots where harmful/toxic particulate matter could accumulate, whereas 3D-1D multiscale ensures realization of lung function at a global (organ) level, e.g. ventilation (flow distribution) at different regions of the lung.

Coupling of structure and function

Yin et al. [49] compared the distributions of outlet velocity and static pressure for three BCs: image-based BC, uniform velocity BC and uniform pressure BC. The distributions of outlet velocity and pressure in Fig. 4(a) obtained from the image-based BC are more heterogeneous than those of the uniform velocity BC in Fig. 4(b) and the uniform pressure BC in Fig. 4(c). In particular, the image-based BC predicts much greater pressure drop at the airways in the left lower lobe (LLL) and right lower lobe (RLL) shown in Fig. 4(a). In contrast, the uniform velocity BC produces the greatest pressure drop in the right middle lobe (RML), whereas the uniform pressure BC fails to capture the pressure variation at different ending airways. Figure 4(d) compares the lobar distributions of air content predicted by the three BCs against the measured values. The distributions predicted by the image-based BC agree well with the measurements. In contrast, both uniform pressure and uniform velocity BCs under-predicted the ventilation to the LLL and RLL, whereas the uniform velocity BC over-predicted the ventilation to the RML.

The implication of the above BC study for regional deposition of particles is significant. For example, Schlesinger et al. [51] used a hollow, silicone rubber cast of the human tracheobronchial tree to study particle deposition in the human lung. The same model was further used to study preferential particle deposition and its implication in bronchogenic carcinoma [52]. The clinical data for cancer sites [53] were adopted for comparison with their experimental data. They found a close correspondence between the particle deposition efficiency and reported cancer locations in the human lungs. However, their experimental setup placed a hollow tree cast inside an artificial thorax chamber [51], which is equivalent to the uniform pressure BC illustrated in Fig. 4. Thus, the lobar flow rate in their experimental study depends on the specific airway cast geometry rather than parenchymal tissue expansion/ventilation. Their tree cast had more branches (thus, higher flow resistance) in the

NIH-PA Author Manuscript

NIH-PA Author Manuscript

NIH-PA Author Manuscript

lower lobes than the upper lobes, resulting in relatively more air, and subsequently more particles, being transported to the upper lobes. This example highlights the importance of accurate representation of BCs, which can only be achieved through coupling airway structure and lung function.

TURBULENCE MODELS AND PARTICLE TRANSPORT

Turbulence models

Due to the glottal constriction, a laryngeal jet is formed at the glottis in the trachea on inspiration [15] as demonstrated in Fig. 5. The jet flow could be transitional or turbulent, depending on the Reynolds number (Re), and propagate deeper into the lungs[29, 54, 55]. There are three major approaches to model turbulent flow: direct numerical simulation (DNS), large-eddy simulation (LES), and Reynolds-Averaged Navier-Stokes (RANS) models. DNS resolves all of the turbulent structures in the flow without using any turbulence model. LES resolves only large-scale energy-containing turbulent structures in the flow, and uses a sub-grid scale model to represent un-resolved small-scale turbulent eddies. RANS resolves only the mean velocity field and parameterizes all turbulent structures. DNS is accurate, but is computationally costly. LES is fairly accurate, and is affordable with today's computing technologies. RANS is inaccurate, but is computationally inexpensive. There are two RANS-based approaches to predict particle transport. One approach is to use the mean velocity fields alone, known as "mean flow tracking" (MFT). The other approach is to generate random turbulent fluctuations based on RANS-predicted mean turbulent kinetic energy (TKE), called "turbulent flow tracking" (TFT). MFT prohibits turbulent mixing of particles, which is numerically equivalent to particle transport in steady laminar flow. Thus, MFT depends on particle release location, which is against the nature of turbulent flow. On the other hand, although TFT attempts to model turbulent mixing, it does not correctly predict turbulent mixing because RANS-predicted mean TKE is inaccurate in both magnitude and distribution. Nonetheless, because of its convenience and inclusion in a wide range of commercial software packages, RANS has been widely used for pulmonary flow simulations as well as studies of particle transport and deposition [56–59].

Several studies have examined the suitability of RANS for airflow and particle simulation. For example, Heenan et. al. [60] investigated both experimentally and numerically the velocity field in an idealized representation of the human oropharynx during steady inspiration, and found that RANS is not adequate to capture the flow structures. Jayaraju et al. [61] found that LES and detached eddy simulation significantly improve the prediction of deposition of particles of 5 μm and smaller in diameter over RANS using both MFT and TFT. Ma and Lutchen [35] reported that the oral deposition predicted by MFT is more accurate than that of TFT. In contrast, van Ertbruggen et al.[8] compared the flow profiles and particle deposition predicted by laminar and RANS models, and found insignificant difference between the two models. They determined the critical Re in their model to be 8,000. Since the maximum Re in their model was 2,500, they concluded that their flow was not turbulent. Their critical Re, however, is over estimated because the critical Re for transition to turbulent flow in a straight pipe[62] is about 2,300 [63]. Furthermore, Dekker [64] studied experimentally the critical velocities in 21 transparent plastic casts of human trachea, and reported a critical Re of 400, and Vétel et al. [65] reported that the laminar flow through a smooth axisymmetric 75% sinusoidal constriction becomes unstable at a critical Re of 400. It is noted that the airway model used by van Ertbruggen et al. [8] did not include the upper airway or the glottal constriction. Lin et al. [15] demonstrated that without including the upper airway in CFD simulation the flow becomes laminar. In more recent studies, Darquenne et al. [66] used the same airway model as van Ertbruggen et al. [8] along with a RANS model to study the relationship between ventilation and transport of particles of size 0.5, 1 and 2 μm, and Lambert et al. [19] studied particle deposition and hot spots for particles of 2.5, 10, and 30-μm

NIH-PA Author Manuscript

NIH-PA Author Manuscript

NIH-PA Author Manuscript

in diameter and the left-right lung particle ventilation asymmetry using LES. Lambert et al. [19] computed particle trajectories in the airways with the Lagrangian tracking algorithm [67, 68]. They found that deposition for 2.5 μm particles is most uniform, whereas 30-μm particles have the highest deposition rate and predominantly deposit in the oral region. One limitation of the above studies is that they were based on static anatomic conditions. Nonetheless, the left-right lung particle ventilation asymmetry predicted by Lambert et al. agrees with the findings of Bennett[69] and Möller et al.[70] who studied in vivo bolus inhalation using gamma camera imaging.

Particle transport by laminar and turbulent flows with different carrier gases

Sandeau et al. [71] used a RANS model to predict flow, pressure drop and particle deposition for air and helium-oxygen mixtures in a human oral extra-thoracic airway model. They found that the pressure drop and particle deposition in the model with helium-oxygen were reduced compared with air. Miyawaki et al. [68] studied the effect of carrier gas properties on distribution of 2.5 μm particles to the left and right lungs, thus the left-to-right-lung (L/R) ratio using LES. They considered five different cases: helium (He), helium-oxygen mixture (He-O_2), helium with a flow ventilation ratio 2:3 to the left and right lungs (He23), air, and xenon-oxygen mixture (Xe-O_2). Except for the case with He23, the CT-measured air ventilation ratio of 0.98 to the left and right lungs specific to this subject was imposed. Given the same flow rate at the mouthpiece inlet in Fig. 6(a) but different gases, the Re values at the trachea for He, He23, He-O_2, Air, and Xe-O_2 cases are about 190, 190, 460, 1300, and 2800, respectively. With increasing Re, the high-speed jet that formed at the glottal constriction was more dispersed around the peripheral region of the jet and its length became shorter. Figure 6(b) shows that in the laminar flow the distribution of particles in the central airways depends on the particle release location at the mouthpiece inlet, whereas in the turbulent flow the particles are well mixed before reaching the first bifurcation and their distribution is strongly correlated with regional ventilation. The implication is that use of RANS models to predict particle transport and deposition would depend on the particle release location, and this is contrary to the nature of turbulent flow.

Discussion and Conclusion

Bridging individual and population scales: Galbán et al.[72] analyzed CT images of 194 chronic obstructive pulmonary disease (COPD) subjects to identify image-based biomarkers that can detect COPD subtypes for individualized medicine, a paradigm built on individual- and population-levels. Similarly, the Severe Asthma Research Program (SARP) studies[73, 74] applied an unsupervised hierarchical cluster analysis to clinical variables of 1,644 patients[74], and selected three most discriminatory variables: baseline FEV_1, maximum FEV_1 and age of onset, to identify five distinct classes of asthma. With this paradigm in mind, the ultimate goal of the aforementioned development of a multiscale framework, which consists of airway geometric modeling, image registration, CFD and hot spot prediction, is to identify new sensitive structural and functional variables at local smaller scales for distinguishing normal and diseased phenotypes. For example, airway structures could be classified into sub-populations by gender, age, and normal/diseased state, e.g. based on airway dimensions (men vs. women; normal vs. asthma), airway wall thickness (normal vs. asthma vs. COPD), branching angles (normal vs. asthma) and branching patterns (trifurcation vs. double bifurcations). Likewise, the registration-derived ventilation and CFD-predicted stress and particle deposition, although heterogeneous, may exhibit similar characteristics in sub-populations (normal vs. asthma vs. COPD). To achieve this goal of identifying sensitive variables, these structural and functional variables must be accurate and detailed at local smaller scales in a subject-specific sense. With sensitive discriminatory variables and associated phenotypes established, one could start to interrogate which phenotype, and

NIH-PA Author Manuscript

NIH-PA Author Manuscript

NIH-PA Author Manuscript

subsequently individuals belong to this phenotype, is more susceptible to environmental risk factors.

Bridging organ and cellular/molecular scales: A critical pathway that bridges the above mechanical model with lung biology is through the mechanosensing capability of the human bronchial epithelial cells (HBE). As Fredberg and Kamm[75] pointed out, the mechanical force exerted on the lung to change lung volume can be transmitted from the organ level down to the levels of tissue, cell and molecule. Airway defense is a multiscale process, involving mechanotransduction to transmit oscillatory mechanical force from macro scale (motion of lung, rib cage, diaphragm, and abdomen) to micro scale (airflow-induced shear stress and tissue stress at a local level), and further translation to biochemical responses via cell signaling to maintain the periciliary liquid (PCL) volume for mucociliary clearance. Based on the HBE cell culture experiments, Tarran *et al.*[76, 77] and Button *et al.*[78, 79] found evidence of the response of epithelial cells to mechanical force. Their studies suggest that the rate of change of mechanical stress is an important stimulus for release of adenosine triphosphate (ATP) into the extracellular PCL environment. ATP, along with its metabolite adenosine, interact with airway epithelial purinergic receptors, to up-regulate transcellular ion and water transports that increase PCL volume and ciliary beat frequency to accelerate mucus transport. Namely, a key component in the airway-defense system is stress-mediated ATP release. Therefore, accurate prediction of ATP release, which up-regulates cell signaling and reaction to maintain PCL volume and hydration, relies upon accurate prediction of stress that triggers its release in a location-specific and state-specific manner. As compared with 1D models, the above 3D multiscale model can capture more realistic local airflow-induced stresses in response to airway abnormalities, such as airway constriction in asthmatics. Another example of the need for 3D models is demonstrated by De Backer et al.[80] who validated CFD-predicted hot spots with those detected by 3D combined single photon emission CT (SPECT) and CT in six patients with mild asthma. They used technetium 99m (^{99m}Tc) pentetic acid as radioaerosols having an average size of 1.32 μm, and found that the hot spots were associated with airway occlusion in both CFD and SPECT/CT results. The interplay between hot spots and increased shear stress associated with constricted airways, and between disturbed PCL water homeostasis (which may subsequently weaken mucociliary clearance) and airway inflammation[81] and remodeling could be better understood if sensitive variables of various types and scales are available.

Other important factors: Although this review is focused on conducting airways, there is a large body of literature on the respiratory airways that is very important in understanding lung physiology and pathophysiology. To name a few, Tsuda et al.[82, 83] studied chaotic mixing of fine/ultrafine particles deep in the pulmonary acinus. Kumar et al.[67, 84] studied the structure and function of the respiratory airways and acini, and found that steady streaming is a key mixing mechanism in acinar flows. Kumar et al.[85] further presented a registration-based multiscale method to obtain a deforming geometric model of mouse acinus based on multi-resolution micro-CT images, which forms a useful tool in tissue mechanical and fluid dynamical studies. Coupling of conducting and respiratory airways for CFD requires some strategies, for example, a multi-stage approach that allows performing CFD analyses in these airway models separately, but mass and flow variables are continuous at joint boundaries. The inflammatory response of the human lungs at cellular and molecular levels involves a variety of mechanisms as reviewed by Moldoveanu et al.[81]. Coupling of the multiscale framework with these mechanisms is essential in understanding lung functions from the perspective of systems biology. It is also worth noting that for enhancement of pulmonary inhaled pharmaceutical drug delivery, Longest et al.[86] proposed a method that combines drug aerosols and hygroscopic excipients to reduce extrathoracic drug loss, but allow growth of particle size for potential targeted drug delivery. For accurate prediction of

NIH-PA Author Manuscript

NIH-PA Author Manuscript

NIH-PA Author Manuscript

hygroscopic particle growth, the thermodynamics, heat and water concentration for the temperature and humidity distributions in the human lungs must be taken into consideration. Under normal conditions the nose heats and humidifies inspired air to close to body temperature and saturated with water vapor, then recovers a large proportion of heat and moisture during expiration. The bronchial airways provide any deficit in heat and moisture when air at less than body temperature and saturated enters the lung, for example, during mouth breathing, breathing at high minute ventilation, or when the normal airway is bypassed by an endotracheal tube. Humidity is supplied to the inspired air from the PCL and mucus. Tawhai and Hunter[87] developed a mathematical model of coupled airway heat and water vapor transfer to predict airway humidity and to study dynamic changes in the PCL throughout the airway tree, which can be further implemented into the 3D computational framework.

In summary, with reduced computational time for image processing, image registration, airway meshing and CFD due to advances in image processing algorithms, computer architectures and parallel computing algorithms and with increased image resolution in space and time due to advances in imaging technologies, the multiscale framework enables building large databases based on sensitive image-based and CFD-derived structural/functional variables for phenotyping. With the assistance of statistical analysis and classification, one could begin to interrogate and identify sensitive variables in sub-populations along with genotypes for early detection of lung disease, moving toward the goal of establishing precision medicine.

Acknowledgments

The authors would like to acknowledge the support of NIH Grants R01-HL-094315 and S10-RR-022421, and the computer time provided by XSEDE.

References

1. Weibel, ER. Morphometry of the human lung. Academic Press; 1963.
2. Balásházy U, Hofmann W. Particle deposition in airway bifurcations—I. inspiratory flow. J Aerosol Sci. 1993; 24(6):745–772.
3. KIM CS, IGLESIAS AJ. Deposition of inhaled particles in bifurcating airway models: I. inspiratory deposition. Journal of Aerosol Medicine. 1989; 2(1):1–14.
4. Comer J, Kleinstreuer C, Hyun S, Kim C. Aerosol transport and deposition in sequentially bifurcating airways. TRANSACTIONS-AMERICAN SOCIETY OF MECHANICAL ENGINEERS JOURNAL OF BIOMECHANICAL ENGINEERING. 2000; 122(2):152–158.
5. Zhang Z, Kleinstreuer C. Effect of particle inlet distributions on deposition in a triple bifurcation lung airway model. Journal of aerosol medicine. 2001; 14(1):13–29. [PubMed: 11495482]
6. Spencer RM, Schroeter JD, Martonen TB. Computer simulations of lung airway structures using data-driven surface modeling techniques. Comput Biol Med. 2001; 31(6):499–511. [PubMed: 11604154]
7. Balásházy I, Hofmann W. Deposition of aerosols in asymmetric airway bifurcations. J Aerosol Sci. 1995; 26(2):273–292.
8. van Ertbruggen C, Hirsch C, Paiva M. Anatomically based three-dimensional model of airways to simulate flow and particle transport using computational fluid dynamics. J Appl Physiol. 2005; 98(3):970–980. [PubMed: 15501925]
9. Horsfield K, Dart G, Olson DE, Filley GF, Cumming G. Models of the human bronchial tree. J Appl Physiol. 1971; 31(2):207–217. [PubMed: 5558242]
10. Gemci T, Ponyavin V, Chen Y, Chen H, Collins R. Computational model of airflow in upper 17 generations of human respiratory tract. J Biomech. 2008; 41(9):2047–2054. [PubMed: 18501360]
11. Schmidt A, Zidowitz S, Kriete A, Denhard T, Krass S, Peitgen HO. A digital reference model of the human bronchial tree. Comput Med Imaging Graphics. 2004; 28(4):203–211.

NIH-PA Author Manuscript

NIH-PA Author Manuscript

NIH-PA Author Manuscript

12. Tian G, Longest PW, Su G, Hindle M. Characterization of respiratory drug delivery with enhanced condensational growth using an individual path model of the entire tracheobronchial airways. Ann Biomed Eng. 2011; 39(3):1136–1153. [PubMed: 21152983]
13. Yeh HC, Schum G. Models of human lung airways and their application to inhaled particle deposition. Bull Math Biol. 1980; 42(3):461–480. [PubMed: 7378614]
14. Allen G, Shortall B, Gemci T, Corcoran T, Chigier N. Computational simulations of airflow in an in vitro model of the pediatric upper airways. J Biomech Eng. 2004; 126(5):604–613. [PubMed: 15648813]
15. Lin CL, Tawhai MH, McLennan G, Hoffman EA. Characteristics of the turbulent laryngeal jet and its effect on airflow in the human intra-thoracic airways. Respir Physiol Neurobiol. 2007 Aug 1; 157(2–3):295–309. PMCID: PMC2041885. [PubMed: 17360247]
16. Freitas RK, Schröder W. Numerical investigation of the three-dimensional flow in a human lung model. J Biomech. 2008; 41(11):2446–2457. [PubMed: 18614172]
17. Wall WA, Gamnitzer P, Gerstenberger A. Fluid–structure interaction approaches on fixed grids based on two different domain decomposition ideas. International Journal of Computational Fluid Dynamics. 2008; 22(6):411–427.
18. De Backer JW, Vos WG, Vinchurkar SC, Claes R, Drollmann A, Wulfrank D, Parizel PM, Germonpré P, De Backer W. Validation of computational fluid dynamics in CT-based airway models with SPECT/CT. Radiology. 2010; 257(3):854–862. [PubMed: 21084417]
19. Lambert AR, O'Shaughnessy P, Tawhai MH, Hoffman EA, Lin CL. Regional deposition of particles in an image-based airway model: Large-eddy simulation and left-right lung ventilation asymmetry. Aerosol Sci Technol. 2011 Jan; 45(1):11–25. PMCID: PMC3034252. [PubMed: 21307962]
20. Stapleton KW, Guentsch E, Hoskinson M, Finlay W. On the suitability of k–< i>ε turbulence modeling for aerosol deposition in the mouth and throat: A comparison with experiment. J Aerosol Sci. 2000; 31(6):739–749.
21. Kleinstreuer C, Zhang Z. Laminar-to-turbulent fluid-particle flows in a human airway model. Int J Multiphase Flow. 2003; 29(2):271–289.
22. Xi J, Longest PW. Transport and deposition of micro-aerosols in realistic and simplified models of the oral airway. Ann Biomed Eng. 2007; 35(4):560–581. [PubMed: 17237991]
23. Cheng K, Cheng Y, Yeh H, Swift D. Measurements of airway dimensions and calculation of mass transfer characteristics of the human oral passage. J Biomech Eng. 1997; 119(4):476. [PubMed: 9407288]
24. Choi J, Xia G, Tawhai MH, Hoffman EA, Lin CL. Numerical study of high-frequency oscillatory air flow and convective mixing in a CT-based human airway model. Ann Biomed Eng. 2010 Dec; 38(12):3550–3571. PMCID: PMC3064990. [PubMed: 20614248]
25. Choi J, Tawhai MH, Hoffman EA, Lin CL. On intra- and intersubject variabilities of airflow in the human lungs. Phys Fluids (1994). 2009 Oct.21(10):101901. PMCID: PMC2774343. [PubMed: 19901999]
26. Yin Y, Choi J, Hoffman EA, Tawhai MH, Lin CL. A multiscale MDCT image-based breathing lung model with time-varying regional ventilation. Journal of Computational Physics. 2012
27. Stanescu D, Clement J, Pattijn J, Van de Woestijne K. Glottis opening and airway resistance. J Appl Physiol. 1972; 32(4):460–466. [PubMed: 5026492]
28. Jan D, Shapiro A, Kamm R. Some features of oscillatory flow in a model bifurcation. J Appl Physiol. 1989; 67(1):147–159. [PubMed: 2759939]
29. Lin C, Tawhai MH, Mclennan G, Hoffman EA. Computational fluid dynamics. Engineering in Medicine and Biology Magazine, IEEE. 2009; 28(3):25–33.
30. Tawhai MH, Pullan A, Hunter P. Generation of an anatomically based three-dimensional model of the conducting airways. Ann Biomed Eng. 2000; 28(7):793–802. [PubMed: 11016416]
31. Tawhai MH, Hunter P, Tschirren J, Reinhardt J, McLennan G, Hoffman EA. CT-based geometry analysis and finite element models of the human and ovine bronchial tree. J Appl Physiol. 2004; 97(6):2310. [PubMed: 15322064]
32. Phalen R, Yeh H, Schum G, Raabe O. Application of an idealized model to morphometry of the mammalian tracheobronchial tree. Anat Rec. 1978; 190(2):167–176. [PubMed: 629400]

NIH-PA Author Manuscript

NIH-PA Author Manuscript

NIH-PA Author Manuscript

33. Sauret V, Halson P, Brown I, Fleming J, Bailey A. Study of the three-dimensional geometry of the central conducting airways in man using computed tomographic (CT) images. J Anat. 2002; 200(2):123–134. [PubMed: 11895110]
34. Fernandez JW, Mithraratne P, Thrupp SF, Tawhai MH, Hunter PJ. Anatomically based geometric modelling of the musculo-skeletal system and other organs. Biomechanics and Modeling in Mechanobiology. 2004; 2(3):139–155. [PubMed: 14685821]
35. Ma B, Lutchen KR. CFD simulation of aerosol deposition in an anatomically based human large–medium airway model. Ann Biomed Eng. 2009; 37(2):271–285. [PubMed: 19082892]
36. Corley RA, Kabilan S, Kuprat AP, Carson JP, Minard KR, Jacob RE, Timchalk C, Glenny R, Pipavath S, Cox T. Comparative computational modeling of airflows and vapor dosimetry in the respiratory tracts of rat, monkey, and human. Toxicological Sciences. 2012; 128(2):500–516. [PubMed: 22584687]
37. Kabilan, S.; Kuprat, AP.; Hlastala, MP.; Corley, RA.; Einstein, DR. A multiscale bidirectional coupling framework. Engineering in medicine and biology society, EMBC; 2011 annual international conference of the IEEE; IEEE; 2011. p. 2414-2417.
38. Wongviriyawong C, Harris RS, Greenblatt E, Winkler T, Venegas JG. Peripheral resistance: A link between global airflow obstruction and regional ventilation distribution. J Appl Physiol. 2012
39. De Backer J, Vos W, Gorle C, Germonpré P, Partoens B, Wuyts F, Parizel PM, De Backer W. Flow analyses in the lower airways: Patient-specific model and boundary conditions. Med Eng Phys. 2008; 30(7):872–879. [PubMed: 18096425]
40. Gillis HL, Lutchen KR. How heterogeneous bronchoconstriction affects ventilation distribution in human lungs: A morphometric model. Ann Biomed Eng. 1999; 27(1):14–22. [PubMed: 9916756]
41. Colletti AA, Amini R, Kaczka DW. Simulating ventilation distribution in heterogenous lung injury using a binary tree data structure. Comput Biol Med. 2011; 41(10):936–945. [PubMed: 21872852]
42. Tawhai MH, Nash MP, Hoffman EA. An imaging-based computational approach to model ventilation distribution and soft-tissue deformation in the ovine lung. Acad Radiol. 2006; 13(1): 113–120. [PubMed: 16399039]
43. Tawhai MH, Nash MP, Lin CL, Hoffman EA. Supine and prone differences in regional lung density and pleural pressure gradients in the human lung with constant shape. J Appl Physiol. 2009; 107(3):912–920. [PubMed: 19589959]
44. Swan AJ, Clark AR, Tawhai MH. A computational model of the topographic distribution of ventilation in healthy human lungs. J Theor Biol. 2012; 300:222–231. [PubMed: 22326472]
45. Christensen GE, Song JH, Lu W, El Naqa I, Low DA. Tracking lung tissue motion and expansion/compression with inverse consistent image registration and spirometry. Med Phys. 2007 Jun; 34(6):2155–2163. [PubMed: 17654918]
46. Yin Y, Hoffman EA, Lin CL. Local tissue-weight-based nonrigid registration of lung images with application to regional ventilation. Proc. of SPIE medical imaging vol. 2009:72620–72621.
47. Yin Y, Hoffman EA, Lin CL. Mass preserving nonrigid registration of CT lung images using cubic B-spline. Med Phys. 2009 Sep; 36(9):4213–4222. PMCID: PMC2749644. [PubMed: 19810495]
48. Yin Y, Hoffman EA, Ding K, Reinhardt JM, Lin CL. A cubic B-spline-based hybrid registration of lung CT images for a dynamic airway geometric model with large deformation. Phys Med Biol. 2011; 56:203. [PubMed: 21149947]
49. Yin Y, Choi J, Hoffman EA, Tawhai MH, Lin CL. Simulation of pulmonary air flow with a subject-specific boundary condition. J Biomech. 2010 Aug 10;43(11):2159–2163. PMCID: PMC3034656. [PubMed: 20483412]
50. Amelon R, Cao K, Ding K, Christensen GE, Reinhardt JM, Raghavan ML. Three-dimensional characterization of regional lung deformation. J Biomech. 2011 Sep-Feb;44(13):2489–2495. [PubMed: 21802086]
51. Schlesinger RB, Bohning DE, Chan TL, Lippmann M. Particle deposition in a hollow cast of the human tracheobronchial tree. J Aerosol Sci. 1977 Dec; 8(6):429–445.
52. Schlesinger RB, Lippmann M. Selective particle deposition and bronchogenic carcinoma. Environ Res. 1978 Jun; 15(3):424–431. [PubMed: 679903]

NIH-PA Author Manuscript

NIH-PA Author Manuscript

NIH-PA Author Manuscript

53. SCHLESINGER RB, LIPPMANN M. Particle deposition in casts of the human upper tracheobronchial tree. Am Ind Hyg Assoc J. 1972; 33(4):237–251. 04/01; 2012/05. [PubMed: 5080675]
54. Tawhai MH, Lin CL. Image-based modeling of lung structure and function. J Magn Reson Imaging. 2010 Dec; 32(6):1421–1431. PMCID: PMC3058528. [PubMed: 21105146]
55. Tawhai, MH.; Lin, C. Comprehensive Physiology. John Wiley & Sons, Inc; 2011. Airway gas flow.
56. Longest P, Holbrook L. In silico models of aerosol delivery to the respiratory tract-development and applications. Adv Drug Deliv Rev. 2011
57. Longest P, Tian G, Walenga R, Hindle M. Comparing MDI and DPI aerosol deposition using *in vitro* experiments and a new stochastic individual path (SIP) model of the conducting airways. Pharm Res. 2012; 29(6):1670–1688. [PubMed: 22290350]
58. Kleinstreuer C, Zhang Z, Donohue J. Targeted drug-aerosol delivery in the human respiratory system. Annu Rev Biomed Eng. 2008; 10:195–220. [PubMed: 18412536]
59. Kleinstreuer C, Zhang Z. Airflow and particle transport in the human respiratory system. Annu Rev Fluid Mech. 2010; 42:301–334.
60. Heenan A, Matida E, Pollard A, Finlay W. Experimental measurements and computational modeling of the flow field in an idealized human oropharynx. Exp Fluids. 2003; 35(1):70–84.
61. Jayaraju S, Brouns M, Lacor C, Belkassem B, Verbanck S. Large eddy and detached eddy simulations of fluid flow and particle deposition in a human mouth–throat. J Aerosol Sci. 2008; 39(10):862–875.
62. Avila K, Moxey D, de Lozar A, Avila M, Barkley D, Hof B. The onset of turbulence in pipe flow. Science. 2011; 333(6039):192–196. [PubMed: 21737736]
63. Pope, SB. Turbulent flows. Cambridge university press; 2000.
64. Dekker E. Transition between laminar and turbulent flow in human trachea. J Appl Physiol. 1961; 16(6):1060–1064. [PubMed: 13884939]
65. Vetel J, Garon A, Pelletier D, Farinas M. Asymmetry and transition to turbulence in a smooth axisymmetric constriction. J Fluid Mech. 2008; 607:351–386.
66. Darquenne C, van Ertbruggen C, Prisk GK. Convective flow dominates aerosol delivery to the lung segments. J Appl Physiol. 2011; 111(1):48–54. [PubMed: 21474695]
67. Kumar H, Tawhai MH, Hoffman EA, Lin CL. Steady streaming: A key mixing mechanism in low-reynolds-number acinar flows. Phys Fluids (1994). 2011 Apr.23(4):41902. PMCID: PMC3094461. [PubMed: 21580803]
68. Miyawaki S, Tawhai M, Hoffman E, Lin C. Effect of carrier gas properties on aerosol distribution in a CT-based human airway numerical model. Ann Biomed Eng. 2012:1–13. [PubMed: 22012081]
69. Bennett WD. Targeting respiratory drug delivery with aerosol boluses. Journal of aerosol medicine. 1991; 4(2):69–78.
70. Möller W, Meyer G, Scheuch G, Kreyling WG, Bennett WD. Left-to-right asymmetry of aerosol deposition after shallow bolus inhalation depends on lung ventilation. Journal of aerosol medicine and pulmonary drug delivery. 2009; 22(4):333–339. [PubMed: 19580369]
71. Sandeau J, Katz I, Fodil R, Louis B, Apiou-Sbirlea G, Caillibotte G, Isabey D. CFD simulation of particle deposition in a reconstructed human oral extrathoracic airway for air and helium–oxygen mixtures. J Aerosol Sci. 2010; 41(3):281–294.
72. Galbán CJ, Han MK, Boes JL, Chughtai KA, Meyer CR, Johnson TD, Galbán S, Rehemtulla A, Kazerooni EA, Martinez FJ. Computed tomography-based biomarker provides unique signature for diagnosis of COPD phenotypes and disease progression. Nat Med. 2012
73. Moore WC, Meyers DA, Wenzel SE, Teague WG, Li H, Li X, D'Agostino R Jr, Castro M, Curran-Everett D, Fitzpatrick AM, Gaston B, Jarjour NN, Sorkness R, Calhoun WJ, Chung KF, Comhair SA, Dweik RA, Israel E, Peters SP, Busse WW, Erzurum SC, Bleecker ER. National Heart, Lung, and Blood Institute's Severe Asthma Research Program. Identification of asthma phenotypes using cluster analysis in the severe asthma research program. Am J Respir Crit Care Med. 2010 Feb 15; 181(4):315–323. PMCID: PMC2822971. [PubMed: 19892860]

NIH-PA Author Manuscript

NIH-PA Author Manuscript

NIH-PA Author Manuscript

74. Jarjour NN, Erzurum SC, Bleecker ER, Calhoun WJ, Castro M, Comhair SA, Chung KF, Curran-Everett D, Dweik RA, Fain SB. Severe asthma lessons learned from the national heart, lung, and blood institute severe asthma research program. American journal of respiratory and critical care medicine. 2012; 185(4):356–362. [PubMed: 22095547]
75. Fredberg JJ, Kamm RD. Stress transmission in the lung: Pathways from organ to molecule. Annu Rev Physiol. 2006; 68:507–541. [PubMed: 16460282]
76. Tarran R, Button B, Picher M, Paradiso AM, Ribeiro CM, Lazarowski ER, Zhang L, Collins PL, Pickles RJ, Fredberg JJ. Normal and cystic fibrosis airway surface liquid homeostasis the effects of phasic shear stress and viral infections. J Biol Chem. 2005; 280(42):35751–35759. [PubMed: 16087672]
77. Tarran R, Button B, Boucher RC. Regulation of normal and cystic fibrosis airway surface liquid volume by phasic shear stress. Annu Rev Physiol. 2006; 68:543–561. [PubMed: 16460283]
78. Button B, Picher M, Boucher RC. Differential effects of cyclic and constant stress on ATP release and mucociliary transport by human airway epithelia. J Physiol (Lond). 2007; 580(2):577–592. [PubMed: 17317749]
79. Button B, Boucher RC. Role of mechanical stress in regulating airway surface hydration and mucus clearance rates. Respiratory physiology & neurobiology. 2008; 163(1):189–201. [PubMed: 18585484]
80. De Backer JW, Vos WG, Vinchurkar SC, Claes R, Drollmann A, Wulfrank D, Parizel PM, Germonpre P, De Backer W. Validation of computational fluid dynamics in CT-based airway models with SPECT/CT. Radiology. 2010 Dec; 257(3):854–862. [PubMed: 21084417]
81. Moldoveanu B, Otmishi P, Jani P, Walker J, Sarmiento X, Guardiola J, Saad M, Yu J. Inflammatory mechanisms in the lung. Journal of inflammation research. 2009; 2:1. [PubMed: 22096348]
82. Tsuda A, Rogers RA, Hydon PE, Butler JP. Chaotic mixing deep in the lung. Proceedings of the National Academy of Sciences. 2002; 99(15):10173–10178.
83. Tsuda A, Laine-Pearson FE, Hydon PE. Why chaotic mixing of particles is inevitable in the deep lung. J Theor Biol. 2011; 286:57–66. [PubMed: 21801733]
84. Kumar H, Tawhai MH, Hoffman EA, Lin C. The effects of geometry on airflow in the acinar region of the human lung. J Biomech. 2009; 42(11):1635–1642. [PubMed: 19482288]
85. Kumar H, Vasilescu DM, Yin Y, Hoffman EA, Tawhai MH, Lin C. Multi-scale imaging and registration-driven model for pulmonary acinar mechanics in the mouse. J Appl Physiol. 2013
86. Longest PW, Tian G, Li X, Son Y, Hindle M. Performance of combination drug and hygroscopic excipient submicrometer particles from a softmist inhaler in a characteristic model of the airways. Ann Biomed Eng. 2012; 40(12):2596–2610. [PubMed: 22820981]
87. Tawhai MH, Hunter PJ. Modeling water vapor and heat transfer in the normal and the intubated airways. Ann Biomed Eng. 2004 Apr; 32(4):609–622. [PubMed: 15117034]

NIH-PA Author Manuscript

NIH-PA Author Manuscript

NIH-PA Author Manuscript

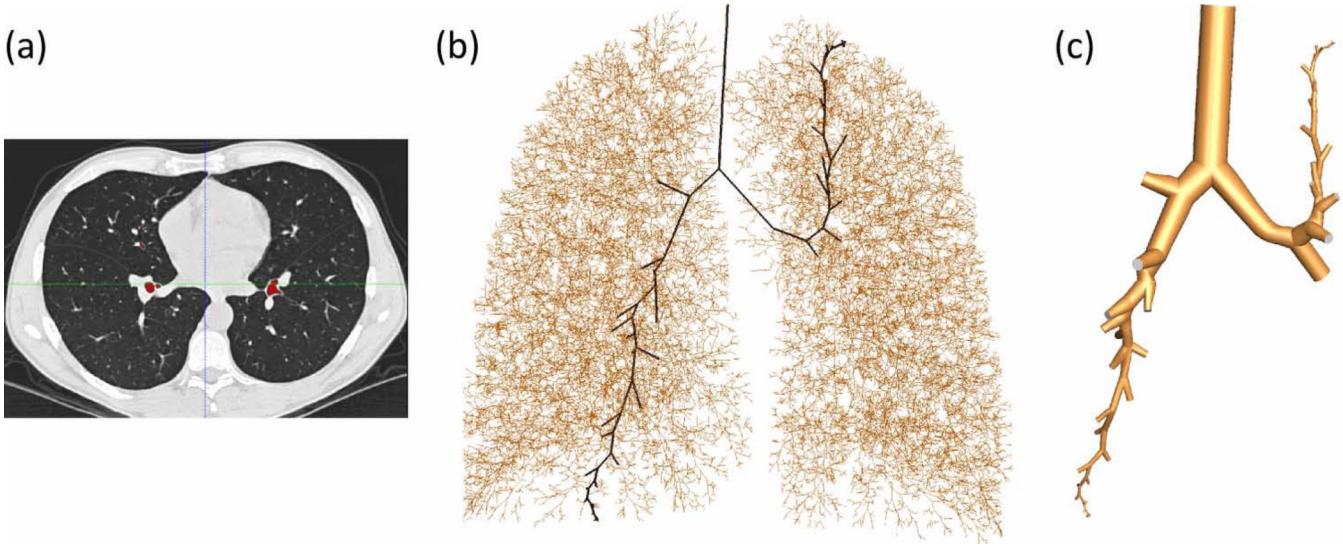

Figure 1.
Mesh generation process: (a) CT image, (b) 1D tree where the black solid lines are paths of interest to the LUL and RLL, (c) 3D geometry generated along the black lines in (b).

NIH-PA Author Manuscript

NIH-PA Author Manuscript

NIH-PA Author Manuscript

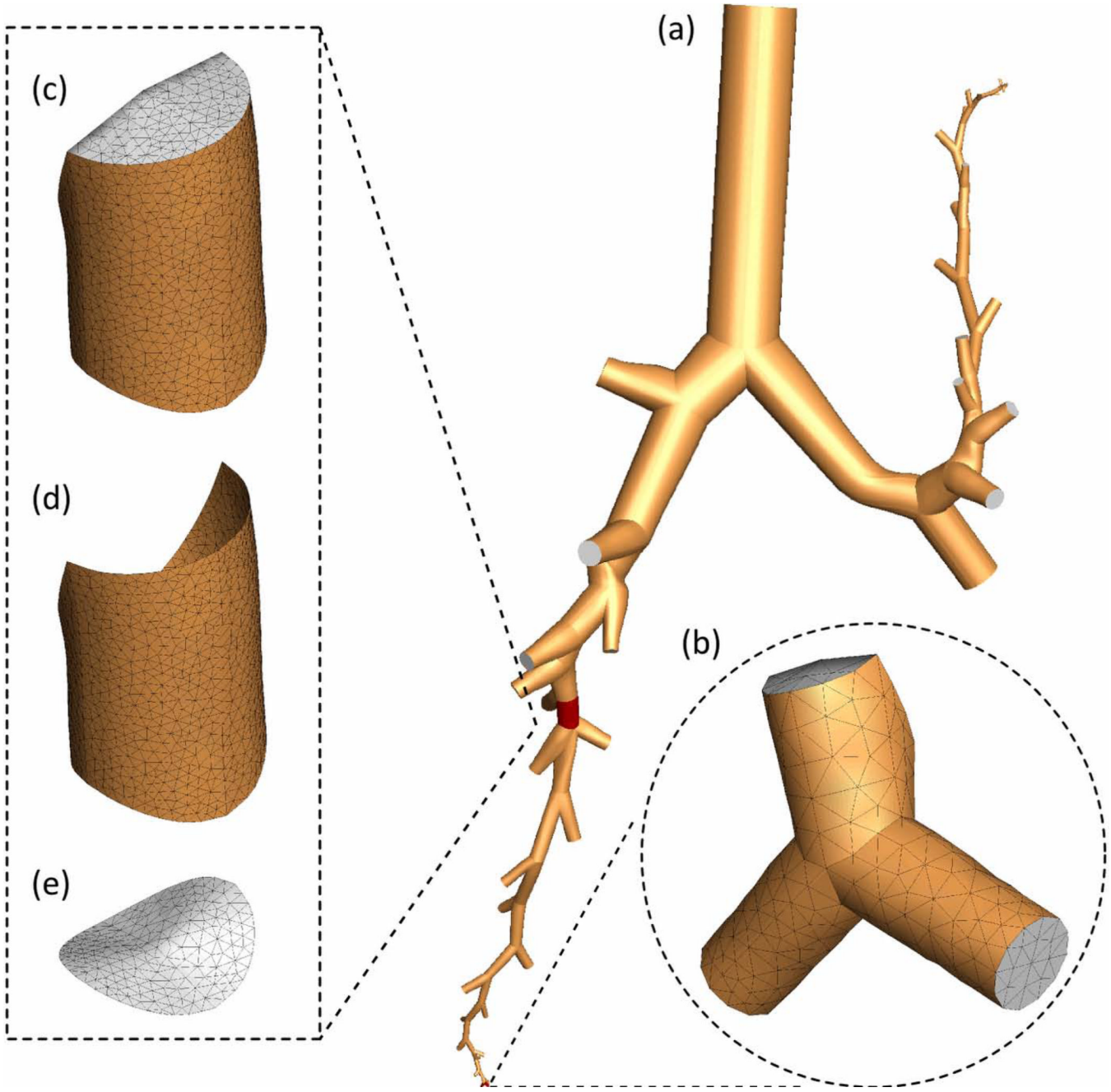

Figure 2.
The 3D CFD grid: (a) 3D geometry, (b) computational grid in terminal airways, (c) airway segment volume, (d) airway segment wall, (e) cross-section.

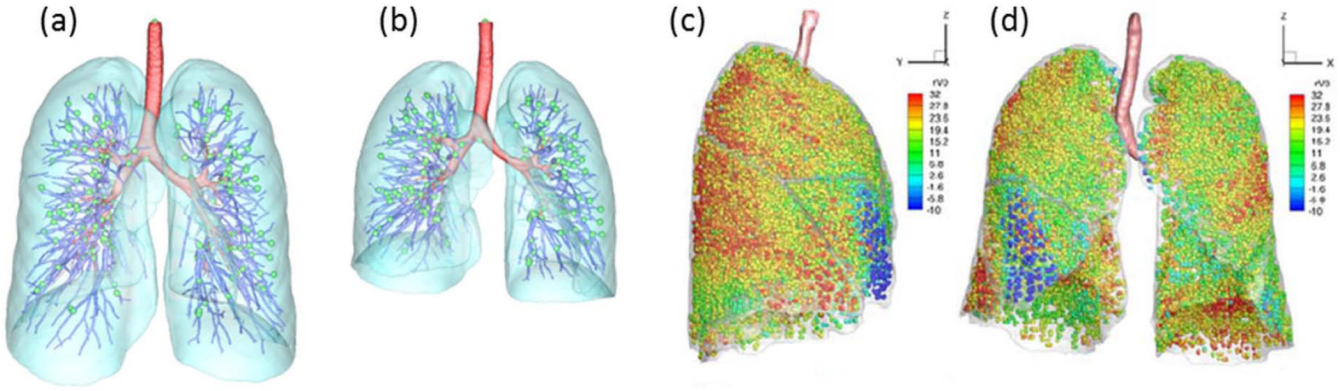

Figure 3.
(a) Reference (TLC) image and (b) floating (FRC) image for one subject. Red, airway tree; blue, vessel tree; cyan, lobes; green spheres, the landmarks at the bifurcations of the vessel tree. Registration-derived heterogeneous regional ventilation: (c) side view, (d) front view.

NIH-PA Author Manuscript
NIH-PA Author Manuscript
NIH-PA Author Manuscript

NIH-PA Author Manuscript

NIH-PA Author Manuscript

NIH-PA Author Manuscript

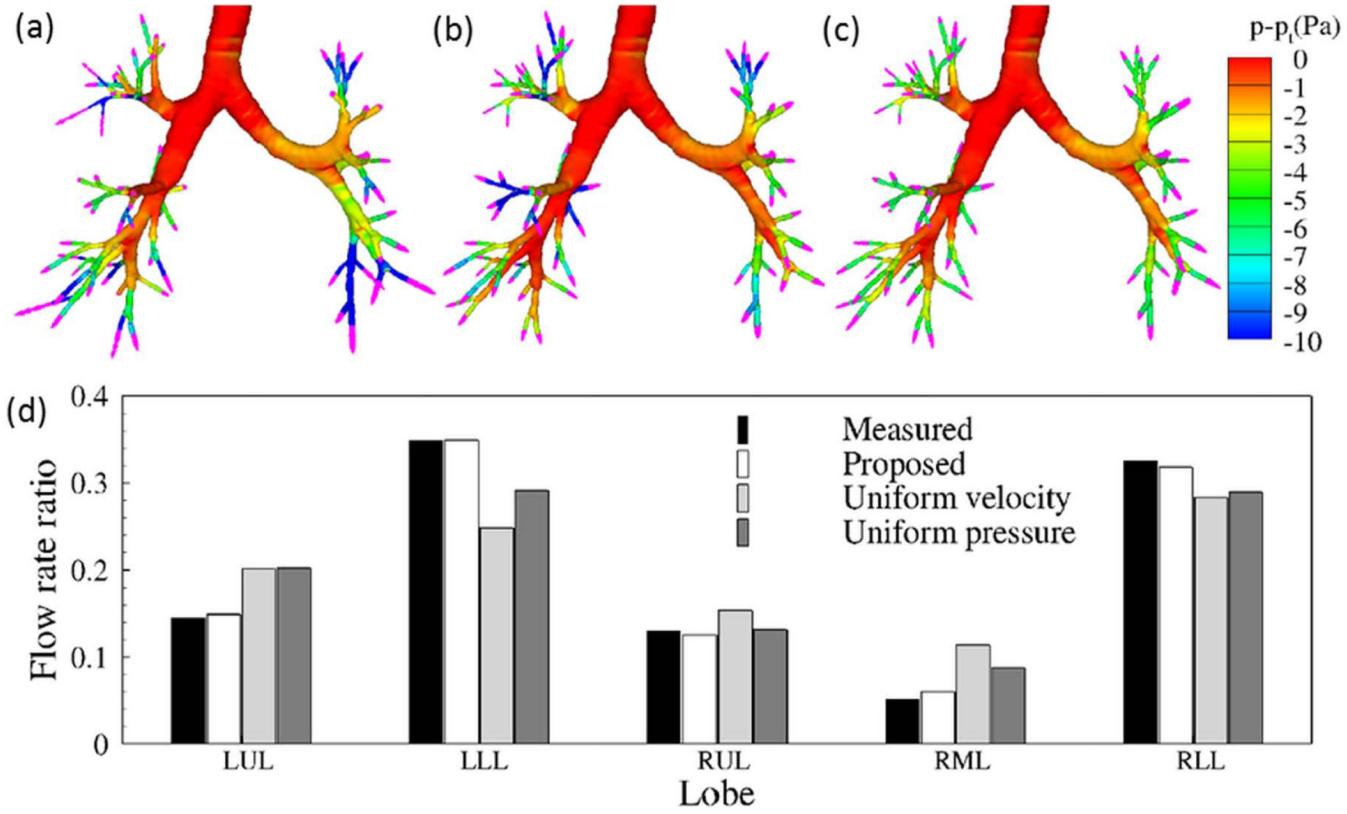

Figure 4.

Top panel: outlet velocity vectors (pink) and pressure contours for the three different outlet BCs: (a) image-based BC; (b) uniform velocity BC; and (c) uniform pressure BC. (d) Lobar distributions of flow rate ratio for the three different outlet BCs. [49]

NIH-PA Author Manuscript

NIH-PA Author Manuscript

NIH-PA Author Manuscript

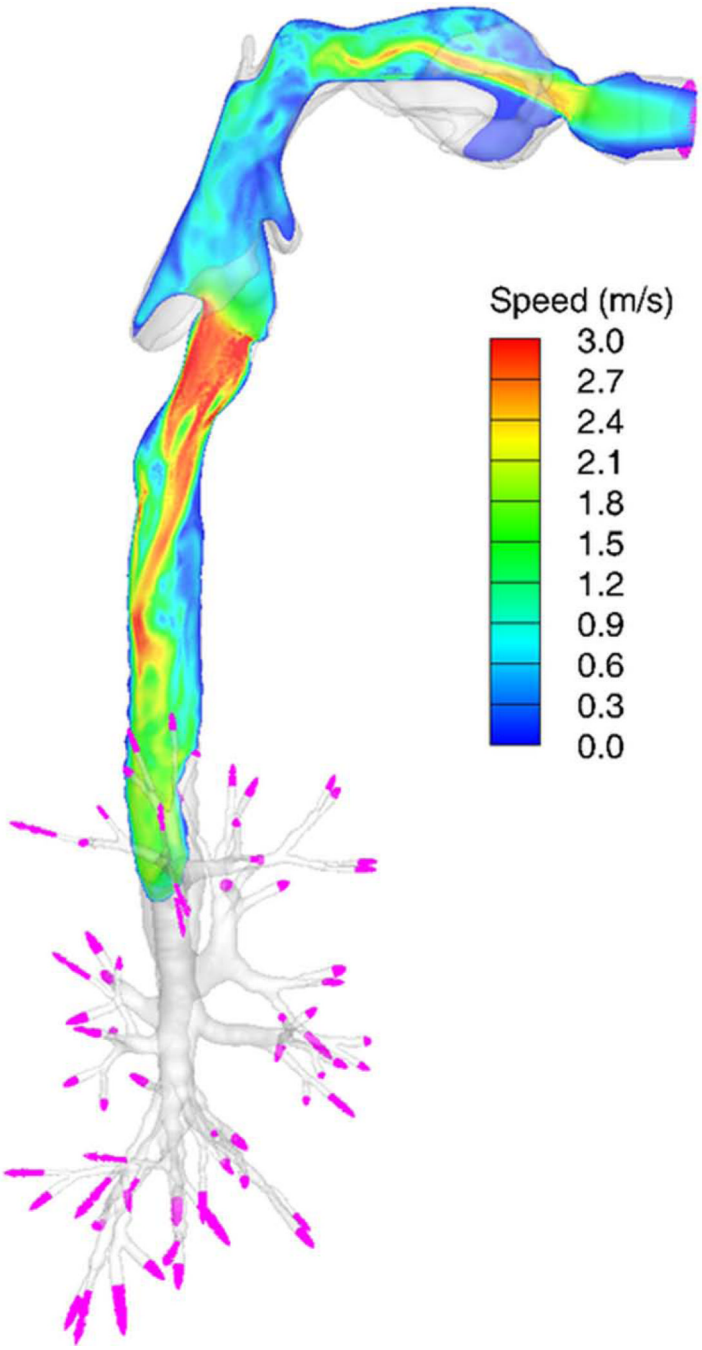

Figure 5.
Contours of speed of inspiratory air in a vertical plane at the middle of the airway model (side view). The velocity vectors at the outlets are displayed in pink. The Re in the trachea is 1,380.

NIH-PA Author Manuscript

NIH-PA Author Manuscript

NIH-PA Author Manuscript

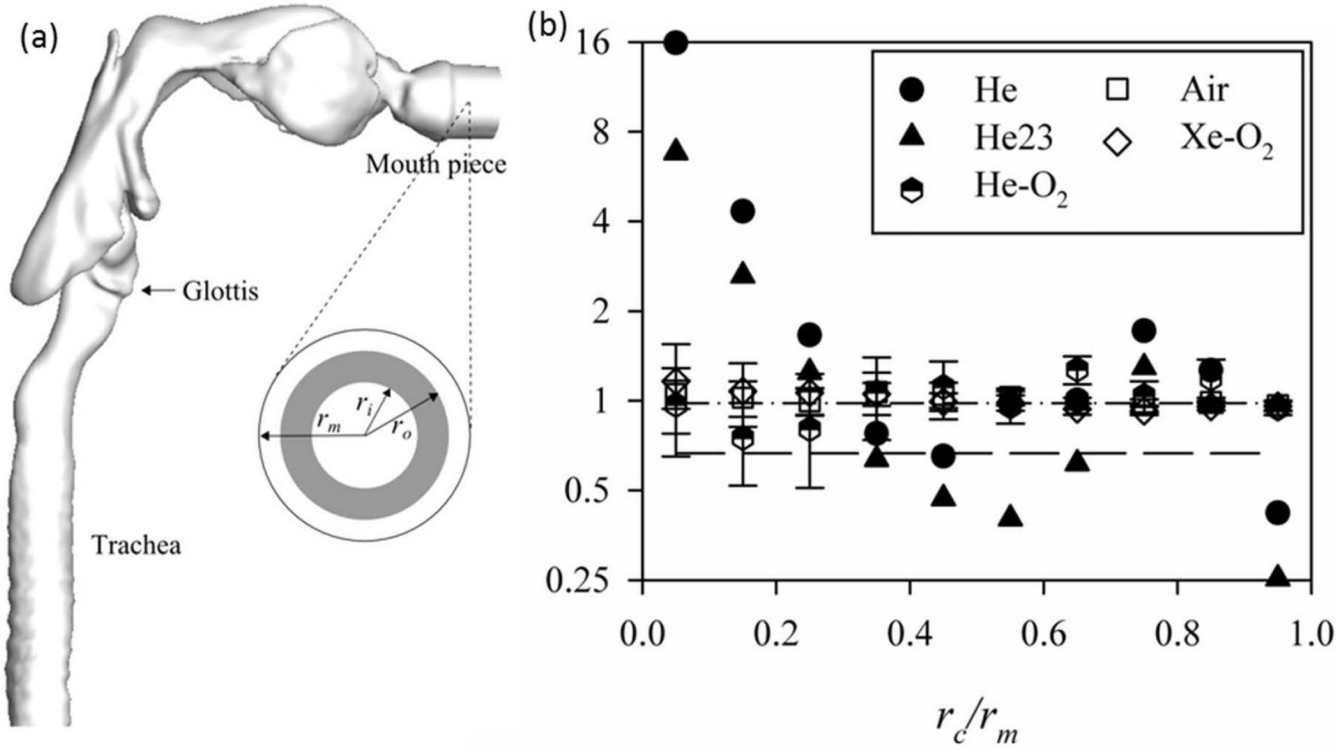

Figure 6.

(a) Side view of a CT-based airway model. The r_m is the radius of the mouthpiece. (b) The left to right lung (L/R) particle ratio as a function of the particle normalized release location at the mouth piece in (a) (the shaded area). $r_c=(r_i+r_o)/2$. He, helium; He23, helium with a ventilation ratio of 2:3; He-O_2, helium-oxygen; Xe-O_2, xenon-oxygen mixture. [68]